

The Spatial Distribution of Atomic Carbon Emission in the Giant Molecular Cloud NGC 604-2

Christopher L. Taylor

*Ruhr-Universität Bochum, Astronomisches Institut
Universitätsstr 150, D-44870 Bochum, Germany
and*

*Five College Radio Astronomy Observatory
University of Massachusetts
Amherst, MA, 01003*

Christine D. Wilson

*McMaster University
Department of Physics and Astronomy
Hamilton, Ontario, Canada, L8S 4M1*

ABSTRACT

We have mapped a giant molecular cloud in the giant HII region NGC 604 in M33 in the 492 GHz $^3P_1 \rightarrow ^3P_0$ transition of neutral atomic carbon using the James Clerk Maxwell Telescope. We find the distribution of the [CI] emission to be asymmetric with respect to the CO J=1 \rightarrow 0 emission, with the peak of the [CI] emission offset towards the direction of the center of the HII region. In addition, the line ratio $I_{[CI]}/I_{CO}$ is highest (~ 0.2) facing the HII region and lowest ($\lesssim 0.1$) away from it. These asymmetries indicate an edge-on morphology where the [CI] emission is strongest on the side of the cloud facing the center of the HII region, and not detected at all on the opposite side. This suggests that the sources of the incident flux creating C from the dissociation of CO are the massive stars of the HII region. The lowest line ratios are similar to what is observed in Galactic molecular clouds, while the highest are similar to starburst galaxies and other regions of intense star formation. The column density ratio, $N(C)/N(H_2)$ is a few $\times 10^{-6}$, in general agreement with models of photodissociation regions.

Subject headings: galaxies: ISM – radio lines: ISM – galaxies: individual (M33) – HII regions: individual(NGC 604) – ISM: molecules

1. Introduction

The fine structure line of atomic carbon at 492 GHz (607 μ m) is one of the important cooling lines of photon dominated regions (PDRs). PDRs form the transition zones between the molecular interstellar medium (ISM) and the atomic ISM, where molecular gas is dissociated by ultraviolet photons from nearby star forming regions. Maps of the distribution of [CI] emission in molecular clouds and on larger scales in nearby galaxies have revealed that it is often cospatial with the emission from

CO (e.g., Keene et al. 1985; Israel, White & Baas 1995), despite the fact that the ionization energy of carbon is very close to the photodissociation energy of CO. From these energy considerations, [CI] would be expected to exist only in a thin layer at the surface of molecular clouds. The similarity between the spatial distributions of CO and [CI] is evidence for a clumpy molecular ISM that allows ultraviolet photons to penetrate into the interiors of molecular clouds (White & Padman 1991).

The ratio of atomic carbon to CO, $N(C)/N(CO)$,

depends on which chemical reactions occur in the PDR, which in turn depends upon the degree of ionization of the gas. When the ionization fraction exceeds a critical value, the gas phase chemistry is dominated by charge transfer reactions with H^+ . These reactions suppress the amount of H_3^+ , the most important species for reactions that destroy atomic carbon. Thus, at high ionization fractions, the abundance of C can remain high, while at lower ionization fractions H_3^+ reactions dominate and C is destroyed (Graedel, Langer & Frerking et al. 1982; Flower et al. 1994). Both UV photons and cosmic rays can influence the ionization fraction. A strong UV field incident upon a molecular cloud will eventually be stopped by the increasing optical depth as the radiation penetrates the cloud. Thus, the distribution of [CI] emission should appear asymmetric. The flux of energetic cosmic rays, on the other hand, will be isotropic within a galaxy and the cosmic rays will be capable of penetrating the entire molecular cloud. If the cosmic rays are a more important source of ionization than the UV flux, the [CI] distribution should appear similar to the CO distribution, with both species tracing the overall distribution of carbon in the ISM.

We present observations of the [CI] line at 492 GHz of the giant molecular cloud (GMC) NGC604-2, in the giant HII region NGC604, which is in the Local Group galaxy M33. By observing a GMC in a nearby galaxy ($D = 0.84$ Mpc; Freedman, Wilson, & Madore 1991), we can map the extent of the cloud in a comparatively short time, and thus determine the spatial distribution of the [CI] emission. NGC604-2 has a molecular mass of $6.3 \times 10^5 M_\odot$, a diameter of ~ 32 pc, and a linewidth of $\sim 11 \text{ km s}^{-1}$ (Wilson & Scoville 1992). It is similar to the larger GMCs in the Milky Way Galaxy. NGC604 is the most luminous HII region in M33, and is the second nearest giant HII region, the nearest being 30 Doradus in the Large Magellanic Cloud. Although these two HII regions are comparable in size, the $\text{H}\alpha$ luminosity of NGC604 is approximately half that of 30 Doradus (Kennicutt 1984). The most important difference between the two regions is the distribution of their ionizing stars: 30 Doradus is dominated by the R136 cluster (Walborn 1991), while in NGC604 the distribution of massive stars is not so concentrated towards the center of the HII re-

gion (Drissen et al. 1993). Hunter et al. (1996) have calculated the average density of O stars in NGC604 to be $0.0018 \text{ stars pc}^{-2}$, 100 times lower than in R136 and more than a factor of 2 lower than the average density over the entire 30 Doradus region.

2. Observations and Data Reduction

We observed the GMC NGC604-2 in the $^3P_1 \rightarrow ^3P_0$ transition of [CI] at 492.2 GHz using the James Clerk Maxwell Telescope (JCMT) on Mauna Kea during 1997 November 21 - 22, 1997 December 12, 1998 December 27 and 1999 July 28. The half power beam width at this frequency is $12''$, so a map was constructed using a grid with $5''$ spacing. The axes of this grid are rotated 45° with respect to the equatorial coordinate system. Calibration observations of W75N and W3(OH) differed from the standard JCMT reference spectra by 20% on 21 November, and by 5% on the other dates, so we adopt as the uncertainty in the absolute calibration a factor of 20%. These reference spectra are available on the JCMT web page: <http://www.jach.hawaii.edu/JACpublic/JCMT>.

The pointing was checked every 1 to 2 hours by observing the planets Mars, Jupiter, and Uranus, and the source NGC7538 IRS1. The pointing of the telescope drifted during the observations, requiring us to correct for this drift. Immediately after a pointing check the pointing accuracy was $1''$ or better, small compared to the beam size. After 1 or 2 hours, the drifting resulted in offsets relative to the intended position that were a significant fraction of the beam. On 1997 November 21, the maximum drift rate measured was $1''$ per hour, while on November 22 the drift reached $1.5''$ per hour, and on December 12 $1.7''$ per hour. For observations taken more than an hour after a pointing check, a correction was applied in the data reduction stage. The altitude-azimuth coordinate system in which pointing is checked rotates with respect to equatorial coordinates through the night, so a systematic drift in alt-az coordinates does not correspond to a constant offset in position in equatorial coordinates. A log of the observed positions, the applied pointing corrections in equatorial coordinates, and the rms noise for the final spectra is given in Table 1.

The data reduction was carried out using the

SPEX package to subtract a linear baseline from each spectrum and average together spectra taken at the same position. The averaged spectra were binned in velocity to a resolution of 3 km s^{-1} to improve the signal-to-noise ratio. To convert the data to the main beam temperature scale, a value of $\eta_{MB} = 0.52$ from the JCMT User's Guide was adopted.

We compare our [CI] observations with the CO $J=1 \rightarrow 0$ emission observed by Wilson & Scoville (1992) using the Owens Valley Millimeter-Wave Interferometer. Prior to comparison, the interferometer data were spatially smoothed to $12''$ resolution. Figure 1 shows the [CI] spectra, compared with spectra from the same positions in the CO $J=1 \rightarrow 0$ line.

3. Results

Table 2 lists the central velocities, full width at half maximum (FWHM), peak temperatures, and integrated intensities for the observed [CI] positions, and for the CO $J=1 \rightarrow 0$ line at those same positions. Wilson (1997) observed [CI] at 492 GHz in NGC 604-2 with a single pointing at the central position, obtaining an integrated flux of $2.8 \pm 0.4 \text{ K km s}^{-1}$. Our new measurement of this position agrees very well with the previous observation. Figure 2 shows our spectra superposed on the full resolution CO $J=1 \rightarrow 0$ map, and Figure 3 shows the spectra superposed on an H α map from the HST archive.

The central velocities of the [CI] line at each location are the same as for the CO $J=1 \rightarrow 0$ line, within the uncertainties. Because of the agreement in central velocities of the two species, it is likely that the [CI] and CO are associated.

Figure 2 shows that the [CI] emission is not distributed symmetrically around the peak of the CO emission. The strongest [CI] emission, measured by the integrated intensity $I_{[CI]}$, occurs to the northwest of the peak of the CO distribution, on the side of the NGC 604-2 that faces the center of the giant HII region. On the opposite side of the cloud, [CI] is not detected.

The line ratio $I_{[CI]}/I_{CO}$ in NGC 604-2 varies from 0.11 to 0.23, with the mean at 0.18 ± 0.02 . The line ratio at the (0,0) position is consistent with that obtained by Wilson (1997). There appears to be a gradient in the line ratio in the cloud,

in the direction facing the center of NGC 604. Figure 4 shows the positions observed in [CI] as in Figures 2 and 3, but with the $I_{[CI]}/I_{CO}$ line ratios and $N(C)/N(H_2)$ column density ratios indicated. The possible gradient is most evident in the line running through the cloud from (0,-5) to (0,10), where the line ratio increases towards the north-west edge of the cloud until the end of the cloud is reached. Our observations do not prove the existence of the gradient, because the difference between positions (0,0) and (0,5) is roughly the same size as the error bars. Such a gradient would be expected, however, due to the higher photodissociation rates at the edge of the cloud.

The column density of atomic carbon may be determined from $I_{[CI]}$ under the assumption that the [CI] emission is optically thin:

$$N(C) = 2 \times 10^{15} (e^{23.6/T_{ex}} + 3 + 5e^{-38/T_{ex}}) I_{[CI]} \quad (1)$$

(Phillips & Huggins 1981), where T_{ex} is the excitation temperature. For T_{ex} we adopt 100 K, which is the kinetic temperature for NGC 604-2 derived by Wilson et al. (1997) from a large velocity gradient (LVG) analysis of CO $J=2 \rightarrow 1$ and $J=3 \rightarrow 2$ lines. In the above equation $N(C)$ does not depend sensitively upon the value of T_{ex} ; in fact, Wilson (1997) remarked that if $T_{ex} = 10 \text{ K}$, then $N(C)$ increases by less than a factor of 2. The column densities we obtain range from $2.3 \times 10^{16} \text{ cm}^{-2}$ to $5.1 \times 10^{16} \text{ cm}^{-2}$.

To derive the column density of atomic carbon relative to molecular hydrogen, we use the CO $J=1 \rightarrow 0$ data to estimate the column density of H_2 . The CO column density cannot be derived from these data because the $^{12}\text{CO } J=1 \rightarrow 0$ line is optically thick, but by using the metallicity dependent CO to H_2 conversion factor of Wilson (1995), we can convert I_{CO} into the H_2 column density. The CO to H_2 conversion factor is 1.5 ± 0.3 times the standard value for the Milky Way Galaxy ($3 \pm 0.3 \times 10^{20} \text{ cm}^{-2} (\text{K km s}^{-1})^{-1}$; Strong et al. 1988). The H_2 column densities vary from $4 \times 10^{21} \text{ cm}^{-2}$ to $8 \times 10^{21} \text{ cm}^{-2}$, giving column density ratios, $N(C)/N(H_2)$, of $\sim 6 \times 10^{-6}$, except at (-5,0), where the ratio is almost a factor of two less.

Table 3 lists the line ratio $I_{[CI]}/I_{CO}$, the atomic carbon column density $N(C)$, and the ratio between carbon and molecular hydrogen column

densities, $N(C)/N(H_2)$.

4. Discussion

4.1. Comparison to Galactic Molecular Clouds

The best comparison to our observations of NGC 604-2 is the sample of four galactic molecular clouds observed by Plume et al. (1999). They mapped the clouds in several lines, including [CI] and ^{13}CO $J=2 \rightarrow 1$. Like us, they mapped most of each cloud, though they obtained a higher physical resolution since their clouds are galactic.

4.1.1. Line Ratios

Plume et al. obtained line ratios of $I_{[CI]}/I_{^{13}CO J=2 \rightarrow 1}$ at various positions in their clouds, with an average line ratio of 0.59 ± 0.19 . For comparison with our data we convert this to $I_{[CI]}/I_{CO}$ (where I_{CO} refers to the ^{12}CO $J=1 \rightarrow 0$ line) using the average line ratio for ^{12}CO $J=2 \rightarrow 1$ to ^{12}CO $J=1 \rightarrow 0$ of 0.7 for the Orion A and B clouds from Sakamoto et al. (1994), and the average value of the ^{12}CO to ^{13}CO $J=2 \rightarrow 1$ line ratio of 5.5 ± 1 measured for the Milky Way by Sanders et al. (1993). The Plume et al. value of $I_{[CI]}/I_{CO}$ becomes 0.08 ± 0.03 , slightly lower than would be allowed by the scatter about our mean value, but consistent within the error bars with some of our individual positions.

If we adopt different, but still reasonable, values for the two line ratios, the results agree with our observations better still. Using the ^{12}CO $J=2 \rightarrow 1$ to ^{12}CO $J=1 \rightarrow 0$ line ratio of 1.3 found near HII regions in Orion instead of the global average, and using the ^{12}CO to ^{13}CO $J=2 \rightarrow 1$ ratio of 4.5 ± 0.7 found by Wilson, Howe & Balogh (1999) for the molecular cloud M17, we find $I_{[CI]}/I_{CO} = 0.17 \pm 0.06$, in good agreement with our observations. Clearly because Plume et al. did not observe ^{12}CO $J=1 \rightarrow 0$, comparisons between our data and theirs will be inexact. We do, however, find a general consistency.

On the edges of the molecular clouds, where the CO is less shielded, Plume et al. find values of the line ratio up to 7 times higher. We see a similar trend in NGC 604-2, but our physical resolution at the distance of M33 is 50 pc, compared to the 1 - 2 pc for Plume et al. Thus, we are averaging over

large areas within the cloud and smoothing away any large contrasts in the line ratio that may exist. Observations with a submillimeter interferometer would help in this case.

Plume et al. find a strong correlation between [CI] line strength and ^{13}CO $J=2 \rightarrow 1$ line strength, and fit both a power-law and linear relation to their data. We can use the ^{13}CO $J=2 \rightarrow 1$ observation by Wilson, Walker & Thornley (1997) to determine if NGC 604-2 follows either relation. The beam size of Wilson et al. is $22''$, so we scale their ^{13}CO $J=2 \rightarrow 1$ intensity by $(22)^2/(12)^2$ to make an approximate correction for the different beam sizes. Using this value in the two fitted relations, we find that either of them reproduces our $I_{[CI]}$ observation at the (0,0) position. The linear relation gives $I_{[CI]} = 2.7 \pm 0.2$, compared to the measured value of 2.8 ± 0.3 . The power law gives 3.0 ± 0.2 . Our data point falls close to both relations in the plot of $I_{[CI]}/I_{^{13}CO J=2 \rightarrow 1}$ versus $I_{^{13}CO J=2 \rightarrow 1}$ in Plume et al., their Figure 10. Both our data point, and the data of Plume et al. are in qualitative agreement with single layer PDR models.

4.1.2. Column Densities

We obtain column densities a factor of 3 to 7 smaller than the typical column densities measured by Plume et al. The difference may be explained by the lower than solar metallicity of NGC 604, or the fact that NGC 604-2 lies in a giant HII region, compared to the more normal galactic star forming regions of the Plume et al. clouds. They find lower column densities at the edges of their clouds, and higher densities at the cloud cores, which we do not, but this is again likely due to our lower physical resolution.

We compare the column density ratio $N(C)/N(H_2)$ in NGC 604-2 with the observations by Plume et al. (1999) and predictions of models by Flower et al. (1994) and Spaans & van Dishoeck (1997). Plume et al. calculate densities of C and ^{13}CO , and the theoretical papers derive column densities of C, ^{12}CO , and ^{13}CO . To convert these CO densities to H_2 densities, we use a $^{13}CO/H_2$ ratio of 1.5×10^{-6} (Bachiller & Cernicharo 1986) and an isotope abundance ratio $^{12}C/^{13}C$ of 62 (Langer & Penzias 1993). These numbers come from molecular clouds relatively close to the solar neighborhood. As a consistency check, we will also convert the Plume et al. ^{13}CO $J=2 \rightarrow 1$ data

to an H_2 column density more indirectly, using the $^{12}\text{CO } J=2 \rightarrow 1$ to $^{12}\text{CO } J=1 \rightarrow 0$ and ^{12}CO to $^{13}\text{CO } J=2 \rightarrow 1$ line ratios discussed in the last section and the Galactic CO to H_2 conversion factor. The uncertainties involved in this indirect determination will be larger than would be the case simply using the Bachiller & Cernicharo density ratio, but it will provide a rough consistency check.

The average $\text{N(C)}/\text{N(H}_2\text{)}$ ratio for the Plume et al. molecular clouds is 2.4×10^{-5} , a factor of four greater than we find for NGC 604-2. From $I_{[\text{CI}]} / I_{\text{CO}} = 0.17$, derived in the previous section, $\text{N(C)}/\text{N(H}_2\text{)}$ is 9×10^{-6} , nearly three times lower than what we found using the Bachiller & Cernicharo density ratio, and more consistent with our number for NGC 604-2. However, as we mentioned, this second method is more indirect, assuming that $^{12}\text{CO } J=2 \rightarrow 1$ to $^{12}\text{CO } J=1 \rightarrow 0$ ratio and the ^{12}CO to $^{13}\text{CO } J=2 \rightarrow 1$ ratio from small Milky Way molecular clouds is applicable to the much larger NGC 604-2, which is located in a giant HII region. It is reassuring that there is an agreement of a factor of three between these two calculations.

The most obvious differences between the Plume et al. clouds and NGC 604-2 are that NGC 604-2 is in a giant HII region, rather than a small HII region, and that NGC 604-2 is more metal poor than the HII region of Plume et al. Stronger dissociating radiation could lead to enhanced C creation through photodissociation. It is also possible that the lower metallicity of NGC 604-2 plays a role; with less C, and therefore less CO, the self shielding of CO against dissociating radiation will be lower, allowing a greater fraction of the existing CO to be dissociated. Of course, lower metallicity also means that the overall abundance of carbon will be lower, so it is not clear to what degree the enhanced photodissociation counters the lower metal abundance. There is a difference in the physical size of the clouds – the Plume et al. clouds are ~ 10 pc in size, compared to ~ 30 pc for NGC 604-2. Perhaps differing $\text{N(C)}/\text{N(H}_2\text{)}$ ratios represent a difference in the distribution of gas in the clouds, with the smaller galactic clouds having lower column density, and hence allowing greater penetration by dissociating radiation.

The models of Flower et al. give $\text{N(C)}/\text{N(H}_2\text{)}$

ranging from $\sim 10^{-4}$ to 10^{-7} . They can easily obtain values consistent with our observations, but the models have at least four free parameters, including the abundances of carbon and oxygen, the visual extinction, A_v , and degree of ionization. With observations of just [CI] and CO we cannot distinguish between their various models. The models of Spaans & van Dishoeck are more constrained because they attempt to model a specific Galactic molecular cloud, S140. Their models assume a clumpy ISM which permits UV radiation to penetrate deep into the cloud. They obtain column density ratios approaching ours for models with low volume filling factors (10% to 30%) and with relatively large clumps (0.4 to 0.6 pc). Of course, S140 is different from NGC 604-2; it is illuminated by a single B0V star, not a giant HII region like NGC 604, so the agreement between the model and our observations should be taken with a grain of salt. However, lacking a detailed model specifically for NGC 604-2, a clumpy ISM would explain our observations.

4.2. [CI] Observations in Other Local Group Galaxies

Stark et al. (1997) have measured the [CI] emission towards two regions within the Large Magellanic Cloud, N 159-W and 30 Dor N. In the latter region, they obtain a $I_{[\text{CI}]} / I_{\text{CO}}$ line ratio of 0.26, twice the average for the Milky Way, but similar to what we have seen in NGC 604. They attribute this large ratio to the lower metallicity of the LMC. Bolatto et al. (2000, in press) find a similarly high line ratio, 0.23 ± 0.03 , in the low metallicity Local Group dwarf irregular galaxy IC 10. Our observations are fairly consistent with this picture; the metallicity of the NGC 604 region is nearly half solar (Vilchez et al. 1988) while the LMC is about one-third solar (8.37; Garnett 1990), and IC 10 is one-fourth solar metallicity (Lequeux et al. 1979).

Figure 5 shows a plot of $I_{[\text{CI}]} / I_{\text{CO}}$ versus metallicity for molecular clouds in Local Group galaxies. The Milky Way Galaxy is also included, with the data on $I_{[\text{CI}]} / I_{\text{CO}}$ coming from the COBE data of Wright et al. (1991). Because COBE did not detect CO $J=1 \rightarrow 0$, we scaled the $I_{[\text{CI}]} / I_{\text{CO } J=2 \rightarrow 1}$ ratio by a typical $^{12}\text{CO } J=2 \rightarrow 1 / ^{12}\text{CO } J=1 \rightarrow 0$ line ratio of 0.7 (Sakamoto et al. 1994). Although only eight points are plotted, the molecu-

lar clouds found near HII regions have consistently higher line ratios than those with no nearby HII regions. This is to be expected if radiation from HII regions is primarily responsible for producing atomic carbon by photodissociation of CO. There also appears to be a trend among the clouds near HII regions for $I_{[CI]}/I_{CO}$ to decrease with increasing metallicity. This trend might be expected if the column density of CO increases with metallicity, thereby more effectively shielding the interiors of the molecular clouds from dissociating radiation. It could also be a result of the metallicity dependence of the CO to H₂ conversion factor – if $I(CI)/N(H_2)$ remains constant, but $I(CO)/N(H_2)$ decreases with metallicity, a similar effect might be observed. More data are needed to confirm these trends.

4.3. The Origin of the [CI] Emission

Figure 2 shows that the spatial distribution of [CI] emission is offset to the northwest relative to the CO. This offset is not due to the pointing problems which were discussed and corrected in Section 2. The center of the giant HII region is northwest of NGC 604-2. This is where most of the O stars are found (Drissen et al. 1993) and hence the source of UV photons. Thus the offset of the [CI] emission is towards the direction from which the photodissociating photons are incident, suggesting an edge-on morphology for the PDR in NGC 604-2.

The fact that [CI] emission is present into the center of the cloud indicates a non-negligible ionization fraction in the cloud’s interior. At low ionizations the gas phase chemistry is dominated by reactions with H_3^+ , which lead to the conversion of carbon into CO (Graedel et al. 1982). One possibility to explain the necessary ionization inside the cloud is penetration by cosmic rays (e.g. Flower et al. 1994). We argue that this mechanism is not likely to be an important one in the case of NGC 604-2 based upon the asymmetric spatial distribution of the [CI] emission. For energies of 10^{18} eV or less, a galactic magnetic field prevents cosmic rays from escaping a galaxy freely (Longair 1994). These cosmic rays spiral around the magnetic field lines, lose their original direction of motion, and become isotropic. Thus ionization from cosmic rays would not be expected to produce the asymmetry in [CI] emission that we see.

In addition, Yang et al. (1996) have identified supernovae driven shells in NGC 604, and the spatial distribution of these shells (and hence the supernovae which could provide the cosmic rays) is not consistent with the [CI] distribution.

We cannot rule out a contribution to the creation of C by cosmic rays, but the lack of [CI] emission at the (0,-5) position, where CO emission is only 25% less than the cloud center (see Figure 1), suggests that any such contribution is small. The (0,5) position lies on the opposite side of the cloud, but facing the center of the giant HII region, and $I_{[CI]}$ here is the strongest we have measured, stronger than at the center of the cloud, although the CO emission is nearly the same as at (0,-5). This result suggests that the atomic carbon is being created by the photodissociation of CO by photons from the massive stars. The penetration of the photons would then be permitted by a clumpy ISM with a moderate or low filling factor (e.g. Stutzki et al. 1988). These photons penetrate partly through the cloud, even to the center, but do not penetrate all the way through, which explains the lack of [CI] emission on the far side.

Churchwell & Goss (1999) argue that the molecular cloud lies behind the HII region, based upon a measurement of extinction towards the cloud that is too low for the molecular mass of the cloud. Our observations do not conflict with this idea, as long as NGC 604-2 is behind the bulk of the ionized gas along the line of sight, but still close enough to the HII region to receive the influx of UV photons that are responsible for dissociating CO and thus producing atomic carbon. Also, if the cloud were too far behind the HII region, then a position like (0,-5) would not be shadowed by the cloud center, and thus would show [CI] emission.

5. Summary

We have mapped [CI] emission in a GMC in the giant HII region NGC 604, the largest HII region in M33. The spatial distribution of the [CI] emission is offset with respect to the CO $J = 1 \rightarrow 0$ emission, with the peak of the [CI] emission sitting in the direction of the center of the HII region. We have argued that this reflects the fact that the massive stars in the HII region produce an intense UV radiation field which photodissociates CO into

C and O and provides the ionization necessary for the chemical reactions which prevent CO from reforming. The fact that the [CI] emission is seen all the way into the center of the molecular cloud can be understood in terms of a clumpy ISM with a moderate or low filling factor which permits deep penetration of UV photons into the cloud. The average line ratio of $I_{[CI]}/I_{CO}$ is 0.18 ± 0.04 , and individual values range from 0.11 to 0.23. Values of 0.1 are commonly seen in Galactic giant molecular clouds, while values of 0.2 are typical for environments of intense star formation activity. We find column density ratios $N(C)/N(H_2)$ of a few $\times 10^{-6}$, which are consistent with numerical models of PDRs.

We thank Gerald Moriarty-Schieven, Henry Matthews and Lorne Avery for performing the remote observing. We also thank the anonymous referee, and the editor, Steve Willner, for helpful comments. The JCMT is operated by the Joint Astronomy Centre on behalf of the Particle Physics and Astronomy Research Council of the United Kingdom, the Netherlands Organization for Scientific Research, and the National Research Council of Canada. The Five College Radio Astronomy Observatory is operated with the permission of the Metropolitan District Commission, Commonwealth of Massachusetts, and with the support of the National Science Foundation under grant AST-9725951.

REFERENCES

- Bachiller, R. & Cernicharo, J. 1986, *A&A*, 166, 283
- Bolatto, A.D., Jackson, J.M., Wilson, C.D. & Moriarty-Schieven, G. 2000, *ApJ*, in press
- Churchwell, E. & Goss, W.M. 1999, *ApJ*, 514, 188
- Drissen, L., Moffat, A.F.J., & Shara, M.M. 1993, *AJ*, 105, 1400
- Flower, D.R., Le Boulrot, J., Pineau des Florêts, & Roueff, E. 1994, *A&A*, 282, 225
- Freedman, W.L., Wilson, C.D. & Madore, B.F. 1991, *ApJ*, 372, 455
- Garnett, D.R. 1990, *ApJ*, 363, 142
- Graedel, T.E., Langer, W.D. & Frerking, M.A. 1982, *ApJS*, 48, 321
- Henry, R.B.C. & Worthey, G. 1999, *PASP*, 111, 919
- Hunter, D.A., W.A. Baum, E.J. O’Neil & Roger Lynds, 1996, *ApJ*, 456, 174
- Israel, F.P., Tilanus, R.P.J. & Baas, F. 1998, *A&A*, 339, 398
- Israel, F.P., White, G.J., & Baas, F. 1995, *A&A*, 295, 599
- Keene, J., Blake, G.A., Phillips, T.G., Huggins, P.J. & Beichman, C.A. 1985, *ApJ*, 299, 967
- Kennicutt, R.C. 1984, *ApJ*, 287, 116
- Langer, W.D. & Penzias, A.A. 1993, *ApJ*, 408, 539
- Lequeux, J., Peimbert, M., Rayo, J.F., Serrano, A. & Torres-Peimbert, S. 1979, *A&A*, 80, 155
- Longair, M.S. 1994, *High Energy Astrophysics* (Cambridge: Cambridge University Press)
- Phillips, T.G. & Huggins, P.J. 1981, *ApJ*, 251, 533
- Plume, R., Jaffe, D.T., Tatematsu, K., Evans, N.J. II, & Keene, J. 1999, *ApJ*, 512, 768
- Sakamoto, S. Hayashi, M., Hasegawa, T., Handa, T. & Oka, T. 1994, *ApJ*, 425, 641
- Sanders, D.B., Scoville, N.Z., Tilanus, R.P.J., Wang, Z., & Zhou, S. 1993, in *Back to the Galaxy*, ed. S.S. Holt & F. Verter (New York: AIP), 311
- Spaans, M. & van Dishoeck, E.F. 1997, *A&A*, 323, 953
- Stark, A.A. et al. 1997, *ApJ*, 480, L59
- Strong, A.W., Bloemen, J.B.G.M., Dame, T.M., Grenier, I.A., Hermsen, W., Lebrun, F., Nyman, L.-Å., Pollack, A.M.T. & Thaddeus, P. 1988, *A&A*, 207, 1
- Vilchez, J.M., Pagel, B.E.J., Diaz, A.I., Terlevich, E. & Edmunds, M.G. 1988, *MNRAS*, 235, 633
- Walborn, N.R. 1991, in *IAU Symposium 148, The Magellanic Clouds*, eds. R. Haynes & D. Milne (Dordrecht: Kluwer), 145
- White, G.J. & Padman, R. 1991, *Nature*, 354, 511
- Wilson, C.D. 1995, *ApJ*, 448, L97
- Wilson, C.D. 1997, *ApJ*, 487, L49
- Wilson, C.D., Howe, J.E. & Balogh, M.L. 1999, *ApJ*, 517, 174
- Wilson, C.D. & Scoville, N. 1992, *ApJ*, 385, 512

Wilson, C.D., Walker, C.E., & Thornley, M.D.
1997, ApJ, 483, 210

Wright, E.L. et al. 1991, ApJ, 381, 200

Yang, H., Chu, Y.-H., Skillman, E.D. & Terlevich,
R. 1996, AJ, 112, 146.

Figure Captions

Fig. 1.— The [CI] spectra of the positions observed in NGC 604-2 (solid line). For comparison, the spectra of CO $J = 1 \rightarrow 0$ are shown (dashed line), divided by 2 to allow plotting with a reasonable scale. The labels indicate the offsets in arcseconds from the central position ($1^h 34^m 33.6^s$, $+30^\circ 46' 48''$). The arrows indicate the directions of north and the center of NGC 604. Not shown are the original observations intended for positions (0,10) and (-5,0). Only the re-observed, correct positions are shown.

Fig. 2.— The [CI] spectra from NGC 604-2 plotted on top of a greyscale image of the OVRO map of CO $J = 1 \rightarrow 0$ emission from Wilson & Scoville (1992). The spectra are plotted at their true positions, but labeled with their intended positions for ease of comparison with Figure 1.

Fig. 3.— The [CI] spectra as in Figure 2, plotted on top of an $H\alpha$ image obtained from the HST archive.

Fig. 4.— The $I_{[CI]}/I_{CO}$ line ratio and $N(C)/N(H_2)$ column density ratio (in italics) for the observed positions.

Fig. 5.— A plot of $I_{[CI]}/I_{CO}$ versus metallicity for extragalactic molecular clouds in the LMC, IC10, M33 (Wilson 1997) and M31 (Israel, Tilanus & Baas 1998). Clouds in the vicinity of HII regions are plotted as filled circles, and clouds with no nearby HII regions present are open circles. The dark cloud D 478 in M31 is plotted at the metallicity extrapolated for its location based upon the metallicity gradient in M31, and the error bars show the range of observed metal abundances. The average line ratio for the Milky Way galaxy (Wright et al. 1991) is plotted at the average metallicity at the solar circle, and the error bar indicating the range of metallicity in the Galaxy (Henry & Worthey 1999).

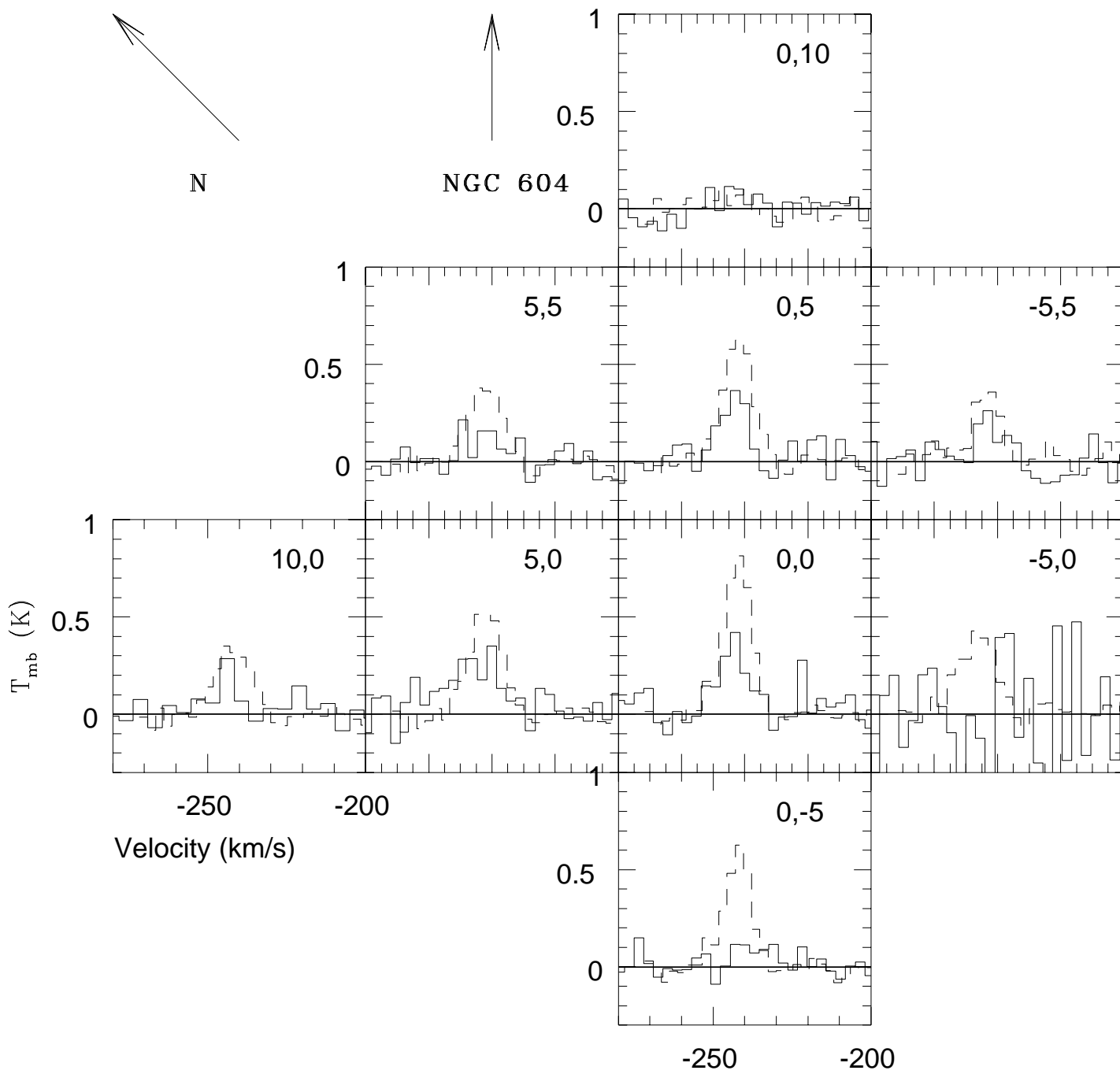


TABLE 1
Log of Observations

Position	Date	Δ Right Ascension* ($''$)	Δ Declination* ($''$)	RMS noise (K)
(0,0)	11/21/97	0.047
(0,5)	11/21/97	0.033
(0,10)	11/21/97	-2.1	-1.4	0.046
(0,10)	12/27/98	0.035
(0,-5)	11/21/97	0.050
(5,0)	11/22/97	0.037
(-5,0)	11/22/97	0.3	-2.2	0.040
(-5,0)	7/28/99	0.078
(-5,5)	11/22/97
(-5,5)	12/12/97	0.046 [†]
(5,5)	11/22/97
(5,5)	12/12/97	0.035 [†]
(10,0)	12/12/97	-4.1	-0.5	0.036

NOTE.— The epoch 2000 equatorial coordinates of the (0,0) position are $1^h 34^m 33.6^s +30^\circ 46' 48''$.

*Applied pointing corrections.

[†]This value is for the average of all spectra observed at this position.

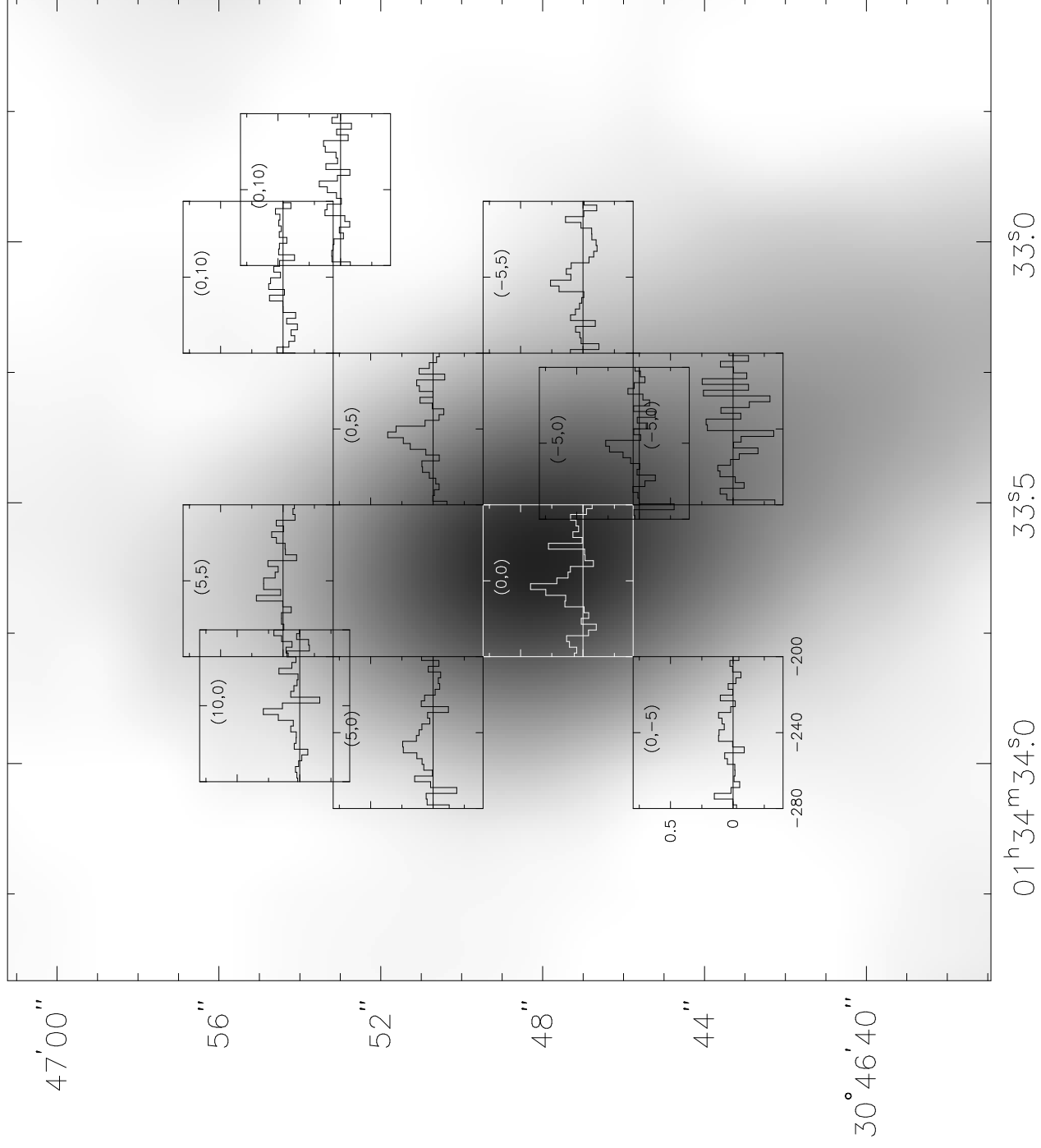


TABLE 2
CI and CO Line Properties

Position	$v_{lsr}(\text{CI})$ (km s^{-1})	$T_{peak}(\text{CI})$ (K)	FWHM(CI) (km s^{-1})	I(CI) (K km s^{-1})	$v_{lsr}(\text{CO})$ (km s^{-1})	$T_{peak}(\text{CO})$ (K)	FWHM(CO) (km s^{-1})	I(CO) (K km s^{-1})
(0,0)	-244.3 ± 1.5	0.42 ± 0.05	7.8 ± 1.5	2.8 ± 0.3	-242.2 ± 0.2	1.7 ± 0.1	10.2 ± 0.5	17.9 ± 3.6
(0,5)	-242.9 ± 1.5	0.36 ± 0.03	10.7 ± 1.5	3.3 ± 0.2	-242.3 ± 0.2	1.5 ± 0.1	10.2 ± 0.5	15.9 ± 3.2
(0,10)
(0,-5)	-242.0 ± 0.3	1.2 ± 0.1	9.5 ± 0.7	12.5 ± 2.5
(5,0)	-244.7 ± 1.5	0.24 ± 0.04	12.4 ± 1.5	3.2 ± 0.3	-242.2 ± 0.4	1.1 ± 0.1	11.7 ± 0.8	13.9 ± 2.8
(-5,5)	-243.1 ± 1.5	0.26 ± 0.05	6.3 ± 1.5	1.6 ± 0.2	-243.5 ± 0.7	0.9 ± 0.2	9.7 ± 1.5	8.8 ± 1.8
(5,5)	-242.2 ± 0.5	0.8 ± 0.1	12.2 ± 1.1	10.4 ± 2.1
(10,0)	-243.1 ± 1.5	0.29 ± 0.04	6.7 ± 1.5	1.9 ± 0.2	-242.2 ± 0.5	0.7 ± 0.1	12.5 ± 1.2	9.5 ± 1.9
(-5,0)	-244.5 ± 0.5	1.0 ± 0.1	12.3 ± 1.2	13.3 ± 2.7
(-5,0)*	-241.5 ± 1.5	0.27 ± 0.04	7.4 ± 1.5	1.5 ± 0.2	-244.1 ± 0.5	1.2 ± 0.3	11.3 ± 1.1	14.2 ± 2.8

NOTE.— The errors quoted for $T_{peak}(\text{CI})$ and $I(\text{CI})$ are from the measurement of the line, and do not include calibration errors. The CI measurements are given in the T_{mb} scale.

* This is the 11/22/97 observation that required a correction for pointing drift.

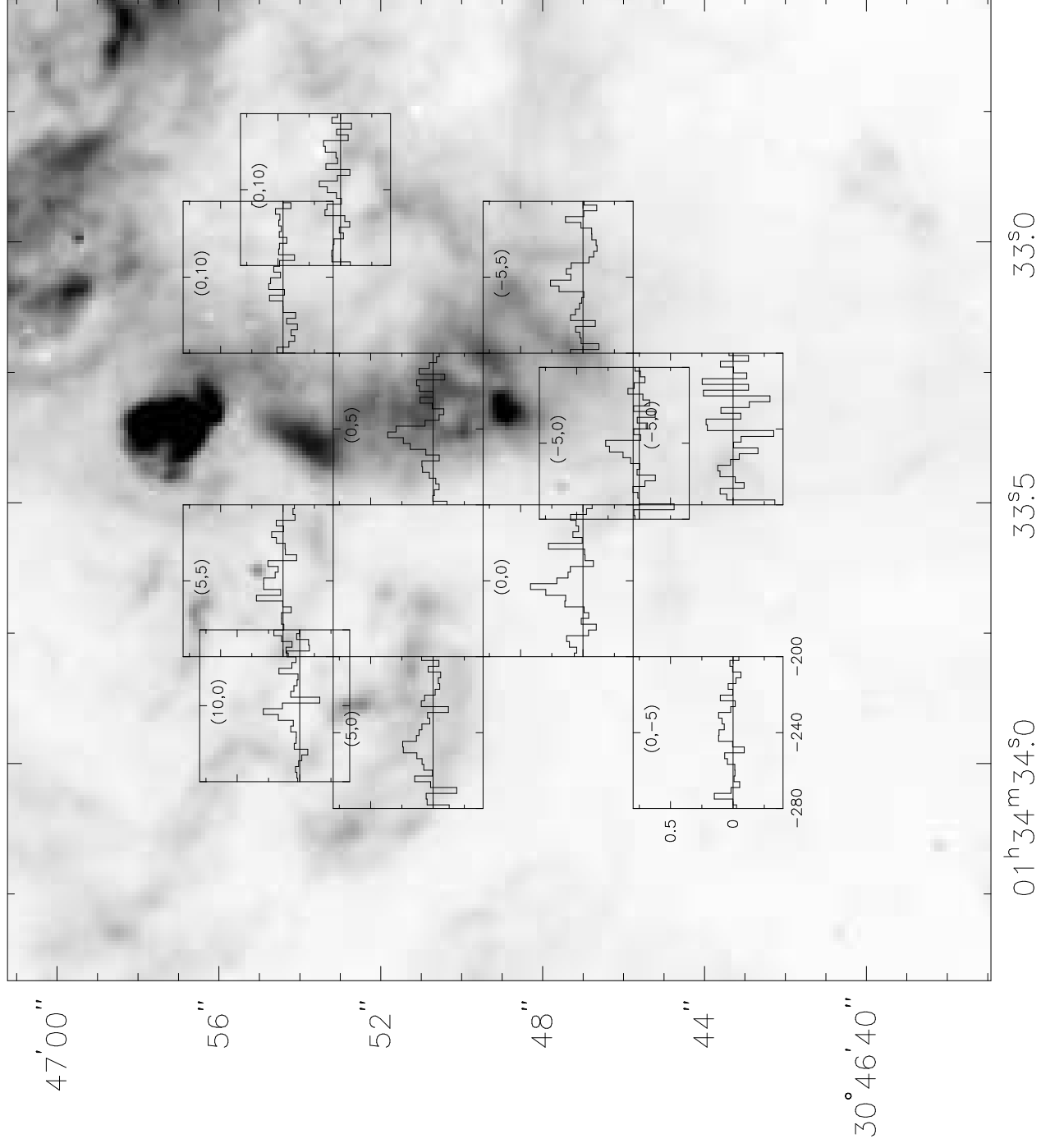


TABLE 3
Line Ratios and Column Densities

Position	$I_{[CI]}/I_{CO}^*$	$N([CI])$ (10^{16} cm^{-2})	$N([CI])/N(H_2)$ 10^{-6}
(0,0)	0.16 ± 0.05	4.3 ± 0.5	5.3
(0,5)	0.21 ± 0.06	5.1 ± 0.3	7.1
(0,10)	...	< 1.9	...
(0,-5)	< 0.11	< 2.1	< 3.8
(5,0)	0.23 ± 0.07	4.9 ± 0.5	7.9
(-5,5)	0.18 ± 0.05	2.5 ± 0.3	6.2
(5,5)	< 0.09	< 1.5	< 3.1
(10,0)	0.20 ± 0.06	2.9 ± 0.3	6.8
(-5,0)	0.11 ± 0.03	2.3 ± 0.3	3.6

NOTE.— Upper limits in [CI] properties are calculated using $3 \times \text{rms}$ and assuming three consecutive channels (9 km s^{-1} total).

*The uncertainties include the 20% calibration uncertainty in each line

